0360-3016/07/$–see front matter

ELSEVIER

doi:10.1016/j.ijrobp.2006.12.068

PHYSICS CONTRIBUTION

FEASIBILITY OF IMAGE REGISTRATION AND INTENSITY-MODULATED RADIOTHERAPY PLANNING WITH HYPERPOLARIZED HELIUM-3 MAGNETIC RESONANCE IMAGING FOR NON–SMALL-CELL LUNG CANCER

ROB H. IRELAND, PH.D.,*§ CHRIS M. BRAGG, M.SC.,†§ MARK MCJURY, PH.D.,§¶
NEIL WOODHOUSE, PH.D.,* STAN FICHELE, PH.D.,* EDWIN J. R. VAN BEEK, M.D., PH.D., F.R.C.R.,*‖
JIM M. WILD, PH.D.,* AND MATTHEW Q. HATTON, M.B.CH.B., F.R.C.P., F.R.C.R.‡

Academic Units of *Radiology, †Medical Physics, and ‡Clinical Oncology, University of Sheffield, Sheffield, United Kingdom; §Department of Radiotherapy Physics, Weston Park Hospital, Sheffield, United Kingdom; ¶Department of Medical Physics, Belfast City Hospital Trust, Belfast, Northern Ireland, United Kingdom; and ‖Department of Radiology, Carver College of Medicine, University of Iowa, Iowa City, IA

Purpose: To demonstrate the feasibility of registering hyperpolarized helium-3 magnetic resonance images (^{3}He-MRI) to X-ray computed tomography (CT) for functionally weighted intensity-modulated radiotherapy (IMRT) planning.

Methods and Materials: Six patients with non–small-cell lung cancer underwent ^{3}He ventilation MRI, which was fused with radiotherapy planning CT using rigid registration. Registration accuracy was assessed using an overlap coefficient, calculated as the proportion of the segmented ^{3}He-MR volume (V_{MRI}) that intersects the segmented CT lung volume expressed as a percentage of V_{MRI}. For each patient, an IMRT plan that minimized the volume of total lung receiving a dose ≥20 Gy (V_{20}) was compared with a plan that minimized the V_{20} to well-ventilated lung defined by the registered ^{3}He-MRI.

Results: The ^{3}He-MRI and CT were registered with sufficient accuracy to enable functionally guided IMRT planning (median overlap, 89%; range, 72–97%). In comparison with the total lung IMRT plans, IMRT constrained with ^{3}He-MRI reduced the V_{20} not only for the well-ventilated lung (median reduction, 3.1%; range, 0.4–5.1%; $p = 0.028$) but also for the total lung volume (median reduction, 1.6%; range, 0.2–3.7%; $p = 0.028$).

Conclusions: Statistically significant improvements to IMRT plans are possible using functional information provided by ^{3}He-MRI that has been registered to radiotherapy planning CT.

Hyperpolarized helium-3 MRI, Image registration, IMRT treatment planning, Non–small-cell lung cancer.

INTRODUCTION

Hyperpolarized noble gas magnetic resonance imaging (MRI) is an emerging technique that enables novel quantitative analysis of pulmonary physiology (1, 2). Although the density of gas introduced into the lungs is low, optical pumping techniques can be used before inhalation to produce extremely high nuclear spin polarization levels that provide a signal size sufficient for MRI. By applying this method with the inert, nonradioactive isotope helium-3 (^{3}He), MR images of *in vivo* lung ventilation and oxygen sensitivity can be obtained with unprecedented spatial and temporal resolution (3, 4). The technique has shown great promise in diseases such as cystic fibrosis, asthma, and emphysema (1).

As demonstrated with other functional imaging modalities, such as emission tomography, image registration of ^{3}He-MRI with anatomic ^{1}H-MRI and X-ray computed tomography (CT) could provide improved clinical interpretation of the functional data, owing to the superior anatomic localization provided by image fusion. In particular, the combination of ^{3}He-MRI and CT for the management of lung cancer patients has the potential to be a clinically important application of ^{3}He-MR image registration.

Radiation pneumonitis

For patients with non–small-cell lung cancer (NSCLC) who are suitable for radiotherapy treatment, functional pul-

Reprint request to: Rob Ireland, Ph.D., Academic Unit of Radiology, University of Sheffield, Sheffield, S10 2JF, UK. Tel: (+44) 1-142711714, Fax: (+44) 1-142265521, E-mail; r.ireland@sheffield.ac.uk

Supported by Spectra Gases (Huntingdon, UK) and Philips Medical Systems (Cleveland, OH). R.I. is funded by the UK Department of Health (N&AHP/PDA/04/012). Weston Park Hospital Cancer Appeal and Sheffield Hospitals Charitable Trust also provided funding. The ^{3}He gas polarizer was loaned from GE Healthcare (Princeton, NJ).

Acknowledgments—The authors thank Patricia Fisher, Sally Fleming, Zead Said, Catherine Anthony, Gillian Brown, Kitty Wilcock, and Anirban Chattopadhyay for their assistance.

Conflict of interest: none.

Received May 24, 2006 and in revised form Dec 18, 2006. Accepted for publication Dec 19, 2006.

monary reserve may be severely reduced because radical radiotherapy will cause damage to noncancerous lung tissue in addition to the intended target volume. Consequently, radiation pneumonitis is the most common dose-limiting complication of radiotherapy (5).

The key to lowering the risk of radiation pneumonitis may be to reduce the dose to healthy regions of lung while maintaining an adequate dose to the tumor. However, this approach requires the healthy (well-ventilated and perfused) lung to be identified. CT images used in conventional radiotherapy treatment planning cannot separate these functioning areas from those that have been previously damaged and contribute little to respiration. Supplementary images of lung ventilation and perfusion are, therefore, required if radiation fields are to be optimized to reduce the dose to healthy lung.

Treatment planning with SPECT

The potential value of incorporating functional information into lung cancer treatment planning has been investigated with single photon emission computed tomography (SPECT) (6–9). However, there are several practical limitations to the use of SPECT for treatment planning, primarily the additional radiation dose and often suboptimal image quality due to difficulties with attenuation correction and image reconstruction. Recently, hyperpolarized ^{3}He-MRI has emerged as an alternative lung ventilation imaging modality that eliminates the need for radioisotopes and has the potential to provide functional information superior to that from SPECT (10).

Although hyperpolarized ^{3}He-MRI has been shown to detect radiation-induced lung injury in rats (11), no previous work has investigated the potential role of *in vivo* ^{3}He-MRI for the assessment and treatment planning of lung cancer patients. For NSCLC patients who require radiotherapy, ^{3}He-MR images of ventilation and function could have a considerable impact on patient management.

Before treatment, many patients have regions of lung with poor ventilation or perfusion that contribute little to effective lung function. By identifying these regions and using the information when planning treatment, ^{3}He-MR images may enable radiation fields to be targeted to limit the dose to the healthy regions of lung, which could reduce the incidence of treatment complications.

In addition, the information provided by ^{3}He-MR functional images will make it possible to calculate dose–volume histograms that are weighted by functional information, which could be a valuable tool for treatment plan analysis (12).

^{3}He-MR image registration

For ^{3}He-MRI to be used in radiotherapy, the images must first be registered with the CT acquired for treatment planning. However, ^{3}He-MR image registration has yet to be widely investigated because the lungs represent a nonrigid system with high mobility and thus present a challenging system for image registration. Image registration of perfusion MRI and ^{3}He-MRI using controlled gas administration has been demonstrated in pigs (13, 14), and a fiducial system for ^{3}He to ^{1}H-MRI registration has been described (15), but *in vivo* studies involving the registration of ^{3}He-MRI to CT have not been previously reported. Therefore, the first objective of this study was to investigate the feasibility of *in vivo* ^{3}He-MR image acquisition and registration to X-ray CT for the management of patients with NSCLC.

IMRT planning

Radiotherapy treatment planning of lung cancer with supplementary functional images has been examined for more than a decade (16, 17). Using conventional treatment-planning techniques on 104 lung cancer patients, Munley *et al.* (18) found that 11% of plans were modified according to SPECT, whereas 48% of plans were considered "potentially modifiable" owing to the identification of lung regions with relatively low perfusion but unable to be utilized for treatment planning without improved planning tools. However, in recent years there have been significant improvements to treatment planning and delivery with the development of intensity-modulated radiotherapy (IMRT). From a study of 41 NSCLC patients, Murshed *et al.* (19) concluded that IMRT planning can significantly improve target coverage and reduce the volume of normal lung irradiated above low doses with a potential 10% reduction in the risk of radiation pneumonitis.

Planning with IMRT involves the specification of a number of constraints, some of which can conceivably be derived from functional information when available. For the case of ^{3}He-MRI, once the images have been registered to planning CT, the ^{3}He-MRI data can then be incorporated into the treatment-planning process. In related SPECT studies, the functional data are incorporated into inverse planning with the aim of reducing the dose to healthy regions of lung and improving the sparing of critical structures (6–8, 16). Therefore, the second objective of this study was to compare IMRT plans constructed with and without constraints derived from the ^{3}He-MRI data.

METHODS AND MATERIALS

NSCLC patients

Patients with NSCLC underwent hyperpolarized ^{3}He ventilation MRI in addition to conventional X-ray CT for radiotherapy treatment planning. All patients gave written informed consent to participate, and the study was approved by the local research ethics committee (NS02-11-1507).

Image acquisition

Hyperpolarized ^{3}He-MR ventilation imaging was performed on a 1.5-T whole body Eclipse system (Philips Medical Systems, Cleveland, OH), which was fitted with a second radiofrequency (RF) amplifier (2 kW; Analogic Corporation, Peabody, MA) and a transmit–receive circuit tuned to 48.5 MHz for ^{3}He (2). Imaging was performed with a flexible twin saddle quadrature transmit–receive RF coil (IGC Medical Advances, Milwaukee, WI). Three syringes that could be filled remotely with ^{3}He or water were placed on the chest to act as fiducial markers (15). Images were

acquired on a flat couch top similar to that used during the acquisition of radiotherapy planning CT. However, accurate reproduction of patient treatment position was not possible owing to the thoracic RF coil, which required the patients to be imaged supine with their arms down.

The ^{3}He images were obtained with a low flip angle, gradient echo acquisition with 112 centric phase encoding views (2), flip angle $\theta = 9°$, 19 coronal slices, 13 mm slice thickness with no gap, field of view = 43 cm, time to echo = 3.4 ms, time to repetition = 6.7 ms, 128 samples, and bandwidth = 16 kHz. Each coronal image was 128 × 128 pixels with 3.3 mm pixel size. The ^{3}He gas (Spectra Gases, Huntingdon, UK) was polarized on site to 30% by optical pumping with rubidium spin exchange apparatus (GE Healthcare, Princeton, NJ). *In vivo* imaging was then performed during a single 14 s breath-hold of a 300 mL ^{3}He/700 mL N_2 mixture inhaled from a Tedlar bag (Jensen Inert Products, Coral Springs, FL) from a starting point of functional residual capacity. No inhalation of room air was permitted. Blood oxygen saturation was monitored with an MRI-compatible pulse oximeter throughout the procedure. Patients were coached in the breathing maneuver and were allowed a trial breath hold with a dummy bag containing room air before imaging. Half-Fourier single shot fast spin echo ^{1}H-MR images were also acquired during the same imaging session with the patients in the same position as during the ^{3}He-MRI.

On the same day, treatment planning transaxial CT was acquired (512 × 512 pixels with pixel size 0.9375 mm) with 5 mm slice thickness (Philips Medical Systems PQS CT). The patients were imaged in the conventional treatment position, which is supine with arms raised above the head while breathing freely.

Image registration

The ^{3}He-MR images were imported into Philips Medical Systems ACQSIM, which interpolated the 19 coronal ^{3}He-MR images to match the voxel size and orientation of the transaxial planning CT. ACQSIM's rigid registration tools were then used to register the ^{3}He-MRI to the planning CT. To assist the manual registration procedure, the fiducial ^{3}He markers were aligned with the external CT contour when possible. Verification of the image registration methodology was performed with a chest phantom that was scanned with the same ^{3}He-MRI and CT imaging protocols as the patients.

Using in-house custom Matlab software (MathWorks, Natick, MA), registration accuracy was assessed using an overlap coefficient (Ω), which is calculated as the proportion of the segmented ^{3}He-MR slice volume (V_{MRI}) that intersects the segmented CT lung slice volume (V_{CT}) expressed as a percentage of V_{MRI}

$$\Omega = 100 \times \frac{V_{MRI} \cap V_{CT}}{V_{MRI}},$$

where the higher the overlap value the better the registration. Segmentation was performed manually by an experienced lung radiotherapy consultant with a suitable windowing of the ^{3}He-MR images that varied from patient to patient because of differences in the signal-to-noise ratio.

The ^{3}He-MR volume may be different than the CT-defined volume, owing to the possibility of ventilation defects detected in the functional images. This is to be expected because many of the patients have a history of heavy smoking and may have regional obstruction from chronic obstructive pulmonary disease evident in their ^{3}He-MRI (20). Hence, the overlap coefficient is a more appropriate measure of ^{3}He-MR to CT registration accuracy than, for example, the intersection-union ratio, which may have been used if the two volumes were expected to be similar.

It is useful to analyze the registration accuracy across the entire lung volume and for individual slices that are the most important when planning treatment. Hence, for each patient, the overlap coefficient was first calculated for each image slice, and then the mean and standard deviation was determined for all slices containing (*1*) CT-defined lung, (*2*) the planning target volume (PTV), and (*3*) the gross tumor volume (GTV).

Table 1. Intensity-modulated radiotherapy planning constraints

Spinal cord	Maximum dose ≤40 Gy
Planning target volume	Mean dose 54 Gy; 90% of volume receiving at least 95% of prescription dose
Normal tissue	Maximum dose ≤54 Gy

IMRT planning

The registered ^{3}He-MRI was segmented in ACQSIM and the contours exported as a DICOM structure set to the Eclipse planning system (Varian Medical Systems, Palo Alto, CA) for IMRT planning.

Functional lung tissue was defined as the intersection of the lung CT volume with well-ventilated lung segmented from the registered ^{3}He images ($V_{MRI} \cap V_{CT}$). Total lung volume included the ipsilateral and contralateral lung but excluded the GTV, which was contoured by an experienced lung radiotherapy consultant. A 5-mm uniform margin was added to the GTV to produce the CTV. The CTV-to-PTV margin was 10 mm in the axial plane and 15 mm in the craniocaudal direction.

Inverse planning for IMRT was performed using the Dose-Volume-Optimizer module of the Eclipse planning system. Plans were produced using five or seven nonopposing, coplanar fields, with the beam angles manually optimized for each patient. The IMRT plans were not used for patient treatment.

For each patient, plans were produced using two distinct sets of dose–volume constraints. In the first set (Plan A), constraints were chosen with the aim of minimizing the volume of lung receiving a dose of ≥20 Gy (V_{20}). In the second set (Plan B), lung constraints were applied to minimize the V_{20} of lung tissue identified on the ^{3}He-MRI as functional. Additional constraints were selected to produce continuous hyperfractionated accelerated radiotherapy (CHART) plans (21) that met the criteria shown in Table 1. Tighter constraints were applied to the PTV to produce homogeneity in the PTV within the International Commission on Radiation Units and Measurements–recommended limits of 95% and 107% where possible.

A full three-dimensional forward dose calculation with inhomogeneity correction was performed for each plan, and dose–volume histograms were produced. For each plan, the following parameters were calculated: (*1*) FLV_{20} (percentage of functional lung receiving ≥20 Gy), (*2*) TLV_{20} (percentage of total lung receiving ≥20 Gy), and (*3*) *MFLD* (mean dose to functional lung).

A measure of the overall quality of the treatment plan, incorporating measures of both target dose and functional lung dose, was given by V_{PTV95}/FLV_{20}, which is the ratio of the percentage volume of the PTV receiving at least 95% of the prescription dose (V_{PTV95}) to the functional lung V_{20}.

In addition, a conformity index (*CI*) was used that accounts for any normal tissue receiving at least 95% of the prescription dose

Table 2. Summary of patient details

Patient no.	Staging	Tumor site	Total lung volume (cm^3)	Functional lung volume (cm^3)	Planning target volume (cm^3)
1	T4N2Mx − IIIB	Right upper lobe	3,930.2	2,246.2	581.0
2	T2N2Mx − IIIA	Right hilum	3,463.6	1,939.3	794.0
3	T4N2Mx − IIIB	Right hilum	4,002.1	2,689.4	747.7
4	T3N2Mx − IIIA	Right upper lobe	5,677.2	3,320.5	759.1
5	T2N0M0 − IB	Left lower lobe	6,120.1	2,899.0	240.3
6	T2NxMx − IB	Left main bronchus	5,825.7	1,057.5	347.4

and for any tissue within the PTV that does not receive this dose (22). The maximal value of the index is unity, when the 95% isodose conforms exactly to the PTV, whereas a value of 0 represents a geographical miss. The index is defined as the product of the fraction of PTV receiving at least 95% of the prescription dose and the ratio of the volume of PTV receiving at least 95% to the volume of tissue receiving at least 95% (the treated volume, V_T):

$$CI = \frac{V_{PTV95}}{V_{PTV}} \frac{V_{PTV95}}{V_T}.$$

Statistical significance of differences between the dose parameters for Plan A and Plan B were calculated using the Wilcoxon signed ranks test.

RESULTS

NSCLC patients

Six male patients consented for the study (Table 2). All patients had histologically proven inoperable NSCLC and had been selected for radical CHART (21). None of the patients had been previously treated with radiotherapy of the thorax. Patients had WHO performance status of 0–2 and forced expiratory volume in 1 s (FEV1) >1.5 L. During ^{3}He-MR imaging, no significant decrease in blood oxygen saturation was observed, and no ill effects were reported after inhalation of the $^3He/N_2$ gas mixture.

Image registration

Lung phantom. For the chest phantom, regions of ^{3}He concentration were well registered to the CT "lung" regions ($\Omega = 100\%$), which demonstrated the validity of the image transfer procedure and the feasibility of ^{3}He-MRI and CT manual rigid registration.

^{3}He-MR and ^{1}H-MR. For *in vivo* data, Fig. 1a demonstrates the complementary information provided by MRI with hyperpolarized ^{3}He. A complete obstruction is evident in the ^{3}He-MR ventilation image from a patient with a tumor in the right upper lobe that is visible on the ^{1}H-MRI (Fig. 1b). The ^{3}He images indicate that the tumor has caused a complete ventilation obstruction of the upper right lung.

^{3}He-MR and planning CT. The registered ^{3}He-MR image displayed with the external, lung, and GTV contours delineated from the planning CT is shown for 2 patients in Fig. 2. In both cases, the ventilation MR images are well registered to the CT lung segments. For Patient 5, the image has been windowed to display 2 fiducials that lie on the external CT contour.

Figure 3 displays the overlap coefficient (Ω) for each image slice, and Table 3 provides the mean and standard deviation of Ω for each patient. According to all the registered images containing CT-defined lung, for Patient 4 ($\Omega = 97.0 \pm 1.9$) and Patient 5 ($\Omega = 96.7 \pm 2.2$) the registration is highly accurate and has low variance. Patients 1, 2, and 6 show good accuracy ($\Omega = 85.5 \pm 15.1$, $\Omega = 89.6 \pm 5.8$,

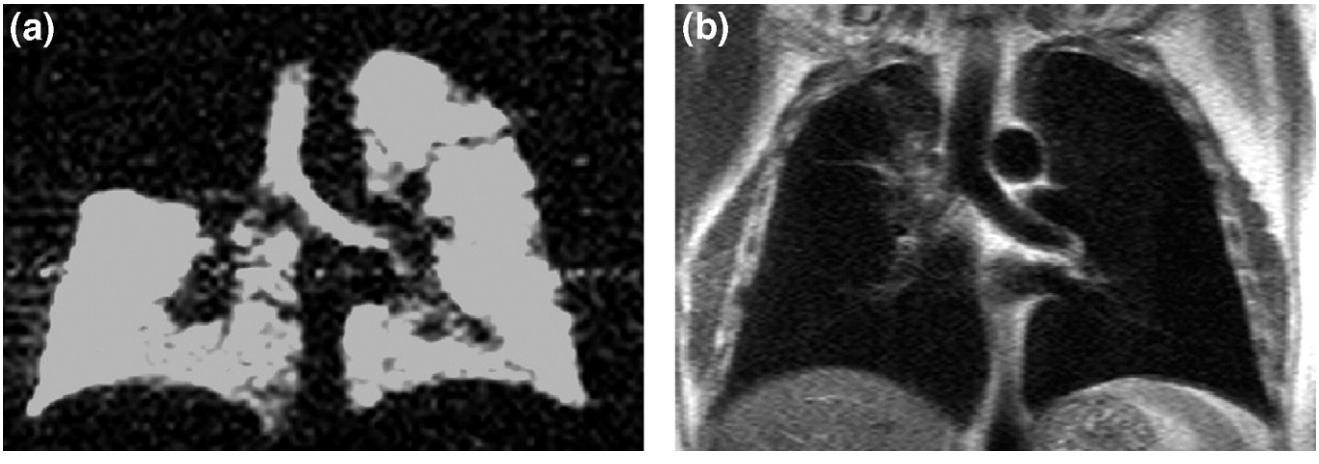

Fig. 1. (a) Hyperpolarized ^{3}He magnetic resonance image exhibiting a complete ventilation obstruction for a patient with a tumor in the upper right lobe. (b) Corresponding ^{1}H magnetic resonance image.

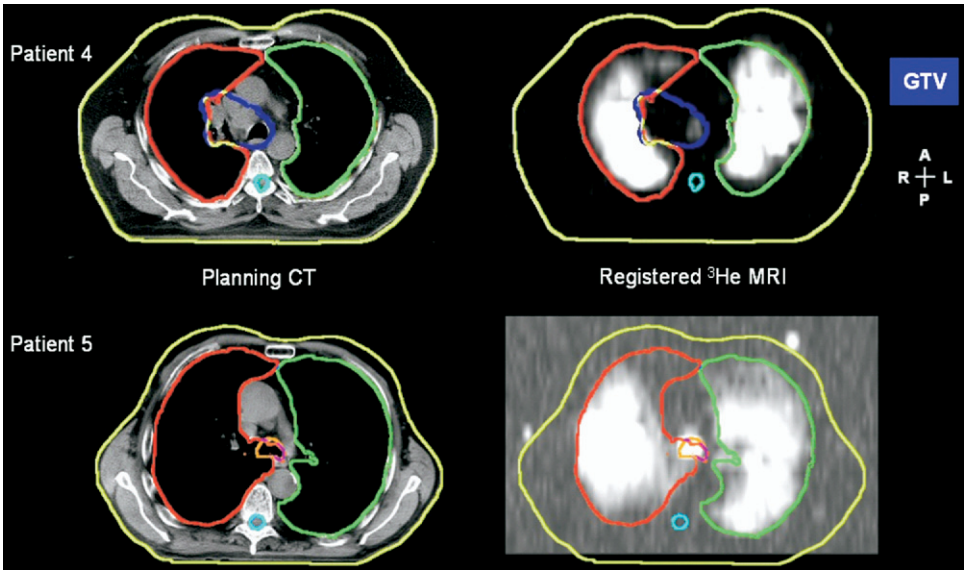

Fig. 2. Sample registered hyperpolarized ^{3}He magnetic resonance image (right) displayed with the external contour, left and right lung and, for Patient 4, the gross tumor volume (GTV) from the transaxial radiotherapy treatment-planning computed tomography (CT) (left).

and $\Omega = 88.2 \pm 8.1$, respectively), whereas Patient 3 exhibits the lowest accuracy and high variability (and $\Omega = 71.9 \pm 14.6$). Similar values are found when Ω is calculated over the registered images containing the PTV or GTV, except for Patient 3, which is 9.8% less accurate over the GTV images compared with overall Patient 3 images containing lung (t test, $p = 0.01$).

Fiducial markers. The markers were not visible for the first 3 patients owing to poor signal-to-noise ratio at the fiducial position due to ^{3}He gas leakage from the syringe. This problem was rectified for the final 3 patients, which allowed the fiducial markers to be visualized on the ^{3}He-MR images (Fig. 2). The markers assisted the manual alignment of the ^{3}He-MRI with the external CT contour, enabling the fusion of the ventilation MR within the CT lung segments.

IMRT planning

The total and functional lung volumes for the patients are shown in Table 2 along with the PTV. Dose–volume parameters achieved by the two sets of optimization constraints are shown in Table 4.

In all patients, the incorporation of ^{3}He-MRI information in the inverse planning process produced improvements in the volume of lung irradiated. This was reflected in reductions not only in FLV_{20} (median reduction, 3.1%; range, 0.4–5.1%; $p = 0.028$) but also in TLV_{20} (median reduction, 1.6%; range, 0.2–3.7%; $p = 0.028$). The *MFLD* was also reduced for each patient when the functional lung was used in the optimization. The lung dose was improved even in patients, such as Patient 5, in whom the optimization using the total lung produced low lung dose statistics.

The improvements in lung dose were sometimes at the cost of deterioration of other aspects of the dose distribution. For example, reductions of more than 3.5% in both FLV_{20} and TLV_{20} and a reduced *MFLD* were seen in Patient 3, but the dose to normal tissue was increased when only functional lung was used in the optimization. This is reflected in the lower *CI* for this patient in Plan B. A lower *CI* was also seen for Patient 5, due predominantly to slightly reduced target coverage, although the PTV dose requirements were met by both plans. In all patients, the overall plan quality measure, V_{PTV95}/V_{20}, was improved when the functional lung was used in the inverse planning process.

The location of the functional lung identified by the ^{3}He-MRI was an important factor in determining the impact of specifically including that tissue in the optimization. In Patient 2, relatively modest improvements were seen in Plan B (for example, a 0.6% reduction in FLV_{20} and a small increase in *CI*). Although 56% of the patient's total lung volume was functional, the majority of that functional tissue lay inferior to the large PTV and so was not in the path of the coplanar beams. As a result, the scope for influencing the volume of functional lung receiving a given dose was limited.

Patient 1 also had a large PTV, extending 13 cm craniocaudally, but in this instance the majority of the functional lung tissue was ipsilateral to and close to the PTV. The two sets of constraints produced plans of a generally similar quality; using the ^{3}He-MRI information in the optimization resulted in similar target coverage, small ($<0.5\%$) reductions in FLV_{20} and TLV_{20}, and identical V_{PTV95}/V_{20}. However, *CI* was lower when the functional lung information was used, reflecting an increased volume of normal tissue receiving at least 54 Gy. This may, in part, be due to the proximity of the functional lung to the PTV—optimizing such that the dose to the functional lung tissue close to the high-dose region is minimized provides a greater challenge

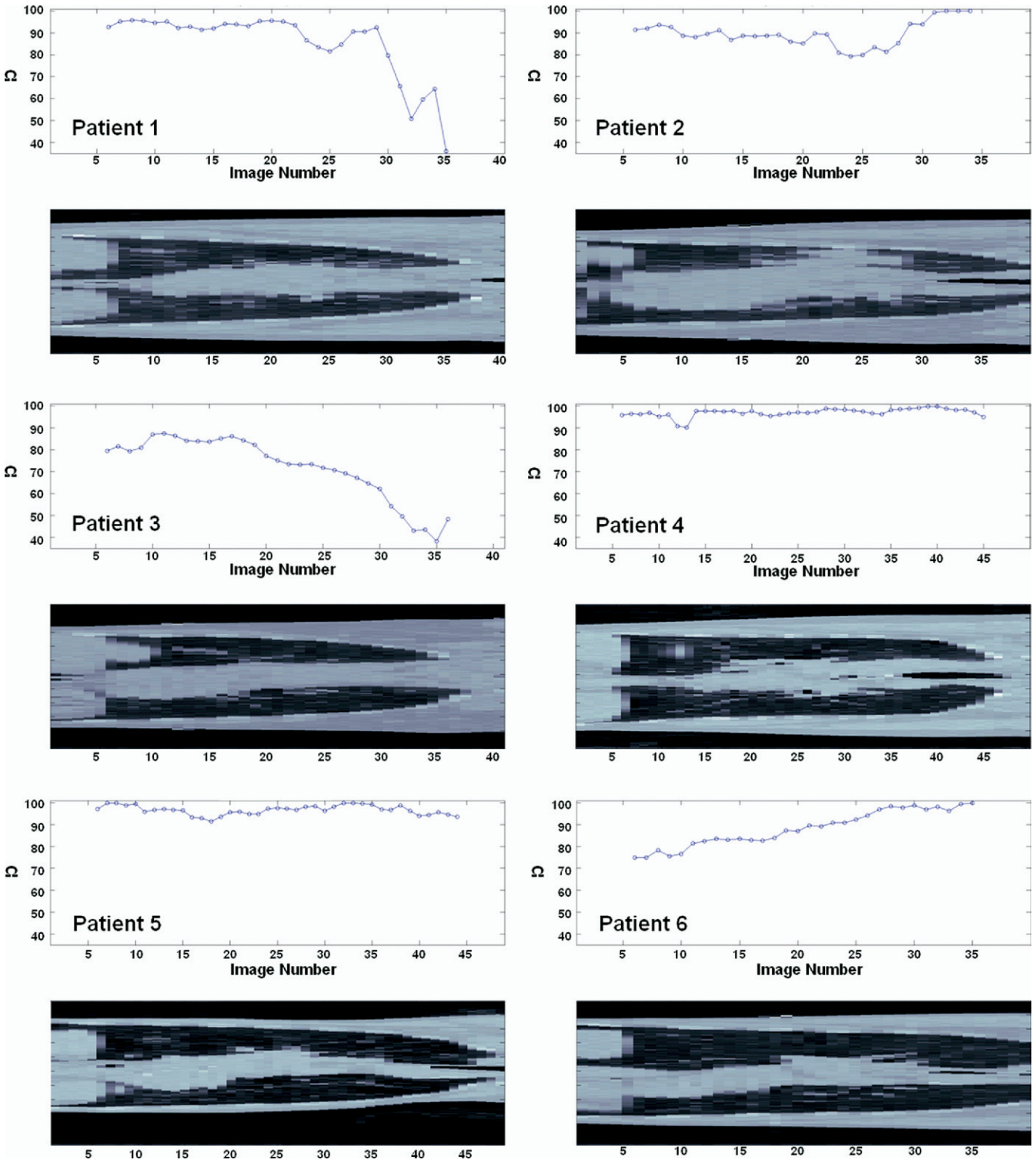

Fig. 3. The overlap coefficient (Ω) to evaluate image registration for all 6 patients displayed with a sample coronal computed tomography slice.

for the inverse planning software. In this instance it seems to have been achieved only at the expense of an increased dose elsewhere.

The PTV of Patient 4 lay close to the spinal cord at some levels. Inverse planning to spare the entire lung consistently produced plans in which the spinal cord dose exceeded tolerance. To maintain an acceptable cord dose, the mean PTV dose was limited to 52.4 Gy, so just 80% of the PTV received at least 95% of the 54-Gy prescription dose. Using only the functional lung in the optimization produced lower spinal cord doses, enabling the desired prescription dose of 54 Gy to be achieved. This was not at the expense of the

Table 3. Mean (SD) of the overlap coefficient used as a measure of registration accuracy calculated for all slices containing CT-defined lung, PTV, and GTV

Patient no.	Within lung images	Within PTV images	Within GTV images
1	85.5 (15.1)	82.8 (16.3)	85.8 (12.2)
2	89.6 (5.8)	89.2 (6.4)	86.4 (4.7)
3	71.9 (14.6)	66.3 (14.7)	62.1 (13.0)
4	97.0 (1.9)	97.7 (1.3)	98.1 (1.0)
5	96.7 (2.2)	96.6 (2.6)	97.0 (2.7)
6	88.2 (8.1)	90.0 (5.8)	89.5 (4.2)

Abbreviations: SD = standard deviation; CT = computed tomography; PTV = planning target volume; GTV = gross tumor volume.

Values are percentages.

lung dose; the FLV_{20} for Plan B was 3.6% lower than that from Plan A, and the *MFLD* was 1.0 Gy lower. If the mean PTV dose in Plan A was increased to 54 Gy such that the cord tolerance was exceeded, these improvements through the use of ^{3}He-MRI information increased to 4.5% and 1.5 Gy, respectively.

The IMRT plans demonstrated the general suitability of inverse planning in the production of clinically acceptable CHART treatment plans. In one instance (Patient 6), the conventional treatment plan produced at the time of the patient's treatment was limited by the proximity of the PTV to the spinal cord, necessitating a compromise in PTV coverage. Both IMRT plans produced met the PTV dose constraints while delivering spinal cord maximum doses well within tolerance (22 Gy and 32 Gy for Plans A and B, respectively).

In just one case (Patient 3), the IMRT plans were clinically unacceptable, because of large hot spots in normal tissue that were present irrespective of the beam arrangement. The delineation of an "avoidance" structure, to which low dose–volume constraints were applied, was of limited help in overcoming this problem. For this patient, whose large PTV extended 16.5 cm in the craniocaudal direction, inverse planning using the Dose-Volume-Optimizer may not be a suitable means of producing a treatment plan. However, the inclusion of noncoplanar beams may assist in reducing the high-dose regions and realizing the potential benefits of sparing the functional lung seen in Plan B.

DISCUSSION

This preliminary work demonstrates the feasibility of acquiring *in vivo* hyperpolarized ^{3}He-MRI suitable for image registration to CT for IMRT treatment planning.

Hyperpolarized helium-3 MRI

The development of MRI for detailed depiction of anatomy in the lungs has been slow when compared with other regions of the body. This is largely owing to the hostile physical environment of the lungs for MRI, namely the low

Table 4. Dose parameters for Plan A (minimizing dose to the total lung) and Plan B (minimizing dose to the functional lung)

	FLV_{20} (%)		TLV_{20} (%)		MFLD (Gy)		V_{PTV95}/FLV_{20}		CI		PTV < 95% (%)		Cord max (Gy)		Vol normal tissue ≥ 54 Gy (%)	
Patient no.	Plan A	Plan B	Plan A	Plan B	Plan A	Plan B	Plan A	Plan B	Plan A	Plan B	Plan A	Plan B	Plan A	Plan B	Plan A	Plan B
1	32.8	32.4	31.4	31.2	15.8	14.9	3.0	3.0	0.85	0.75	2.2	4.1	39.5	39.6	0.09	0.35
2	19.4	18.8	23.2	22.8	12.3	12.2	4.6	4.8	0.79	0.82	9.9	8.9	35.7	36.5	0.16	0.13
3	28.1	24.3	27.6	23.9	13.3	12.5	3.5	3.9	0.86	0.74	2.2	5.2	38.1	40.0	0.17	0.47
4	27.1	23.5	27.1	24.7	14.2	13.2	3.0	4.1	0.76	0.85	18.8	3.4	40.0	40.0	0.02	0.10
5	7.6	5.0	11.7	9.0	5.2	5.0	12.9	18.9	0.86	0.79	2.6	5.2	25.8	30.1	0.01	0.07
6	33.9	28.8	19.0	18.3	16.3	14.0	2.9	3.4	0.85	0.88	1.4	2.4	22.0	32.4	0.07	0.05
Median	27.6	23.9	25.2	23.4	13.8	12.9	3.3	4.0	0.85	0.81	2.4	4.6	36.9	38.1	0.08	0.12
p (Wilcoxon test)	0.028		0.028		0.028		0.043		0.462		0.463		0.043		0.116	

Abbreviations: FLV_{20} = percentage of the functional lung receiving ≥20 Gy; TLV_{20} = percentage of the total lung receiving ≥20 Gy; MFLD = mean dose to the functional lung; V_{PTV95}/FLV_{20} = ratio of the percentage volume of the planning target volume (PTV) receiving at least 95% of the prescription dose (V_{PTV95}) to the functional lung V_{20}; CI = conformity index; PTV <95% = percentage of the PTV receiving less than 95% of the prescribed dose; Cord max = maximum spinal cord dose; Vol normal tissue ≥ 54Gy = percentage of the normal tissue (non-PTV) receiving ≥54 Gy.

proton density and high magnetic field inhomogeneity. Thus, ^{1}H-MRI has provided some limited anatomic information on lung parenchyma at the field strengths that are used routinely (1.5 T). More widespread in clinical radiologic practice is the use of MRI in assessing pulmonary circulation through perfusion and angiography techniques (23). In recent years, the emergence of hyperpolarized noble gas MRI has led to increased interest in the role of MRI for pulmonary assessment because hyperpolarized ^{3}He can provide novel functional information at high spatio-temporal resolution. Helium-3 imaging is safe, noninvasive, and reproducible and does not involve the use of ionizing radiation (1). As an emerging technology, implementation of ^{3}He imaging can be expensive and is currently available at a small number of centers. However, the problems of cost and access may be addressed by the distribution of polarized gas from a central production facility to a large geographic region (24) and by the advent of new clinical whole body scanners capable of multinuclear imaging.

Image registration

Quantification of registration accuracy is a difficult problem. In this study, a measure of overlap is used to provide a measure of registration accuracy. With improved image quality it may become possible to also quantify the registration using anatomic landmarks. Across all 6 patients there was a variable pattern of registration accuracy measured by the overlap coefficient (Fig. 3). However, ^{3}He-MRI and CT were registered with sufficient accuracy to enable functionally guided IMRT planning (median overlap, 89%; range, 72–97%). For Patients 1 and 3, registration accuracy decreased toward the apex of the lungs. For Patient 2, the accuracy dipped toward the middle of the lung. Similarly, a small decrease was observed for Patient 4, but otherwise accuracy was consistently high as was the case for Patient 5. For Patient 6, registration accuracy improved from lower to upper lung.

The example fused images in Fig. 2 were created using a rigid transformation, which is the most commonly used method of image registration. However, there are a number of potential limitations with this approach when applied to lung. First, the ^{3}He-MRI and CT images were acquired with different breathing schemes. Treatment at our institution is planned on CT acquired while the patient is breathing freely. However, ^{3}He-MRI necessitates the use of a breath-hold, and this difference could lead to differences in lung morphology between the two sets of images. Furthermore, the coil used for ^{3}He-MRI precludes the simulation of treatment position while acquiring the ventilation images. Considering the potential problems in this initial study, the application of rigid registration of ^{3}He-MRI and CT was promising because it was possible to register the edges of ventilation images with reasonable accuracy as quantified by the overlap coefficient. Improvements to the methodology, such as the use of ventilation and perfusion ^{3}He-MRI (4), breath-hold CT, treatment position ^{1}H MRI, and nonrigid registration (25, 26) are being explored in a follow-up study that is currently underway.

Treatment planning

Image registration of the ventilation ^{3}He-MRI to CT enabled the functional lung to be taken into account when treatment planning with IMRT, and all plans satisfied the spinal cord dose constraint. When minimizing the dose to total lung (Plan A), V_{20} (median, 25%; range, 12–31%) was comparable to other reported values, such as those reported by Murshed *et al.* (19) (median, 25%; range, 13–43%).

In all patients, optimizing with the aim of reducing V_{20} for functional lung (Plan B) reduced V_{20} not only for functional lung (median reduction, 3.1%; range, 0.4–5.1%; Wilcoxon $p = 0.028$) but also for total lung volume (median reduction, 1.6%; range, 0.2–3.7%; Wilcoxon $p = 0.028$). Functional lung dose was also improved in all patients (median reduction, 0.9 Gy; range, 0.1–2.3 Gy; Wilcoxon $p = 0.028$), and an improvement in plan quality index, V_{PTV95}/V_{20}, was achieved across all 6 patients when optimizing to only functional lung (median increase, 0.45; range, 0–6; Wilcoxon $p = 0.043$). The differences in conformity index were less consistent: Patients 1, 3, and 5 showed an improved degree of dose conformity to the PTV, whereas the other 3 patients had a less well conformed high-dose region. In the patients for whom *CI* was better when the total lung was included in the optimization, the improved conformity was a result of a lower volume of normal tissue receiving 95% of the prescription dose.

CONCLUSIONS

This study has demonstrated that hyperpolarized ^{3}He-MRI can be registered to radiotherapy planning CT. Using the information provided by the registered ^{3}He images, statistically significant improvements to functionally guided IMRT plans were demonstrated for the V_{20} for the total and functional lung, in addition to the mean lung dose to the functional lung.

REFERENCES

1. van Beek EJ, Wild JM, Kauczor HU, *et al.* Functional MRI of the lung using hyperpolarized 3-helium gas. *J Magn Reson Imaging* 2004;20:540–554.
2. Wild JM, Woodhouse N, Paley MN, *et al.* Comparison between 2D and 3D gradient-echo sequences for MRI of human lung ventilation with hyperpolarized 3He. *Magn Reson Med* 2004;52:673–678.
3. Moller HE, Chen XJ, Saam B, *et al.* MRI of the lungs using hyperpolarized noble gases. *Magn Reson Med* 2002;47:1029–1051.
4. Wild JM, Fichele S, Woodhouse N, *et al.* 3D volume-localized pO2 measurement in the human lung with 3He MRI. *Magn Reson Med* 2005;53:1055–1064.
5. Rodrigues G, Lock M, D'Souza D, *et al.* Prediction of radia-

tion pneumonitis by dose-volume histogram parameters in lung cancer: A systematic review. *Radiother Oncol* 2004;71:127–138.
6. Christian JA, Partridge M, Nioutsikou E, *et al.* The incorporation of SPECT functional lung imaging into inverse radiotherapy planning for non-small cell lung cancer. *Radiother Oncol* 2005;77:271–277.
7. Miften MM, Das SK, Su M, *et al.* Incorporation of functional imaging data in the evaluation of dose distributions using the generalized concept of equivalent uniform dose. *Phys Med Biol* 2004;49:1711–1721.
8. Seppenwoolde Y, Engelsman M, De Jaeger K, *et al.* Optimizing radiation treatment plans for lung cancer using lung perfusion information. *Radiother Oncol* 2002;63:165–177.
9. Marks LB, Munley MT, Spencer DP, *et al.* Quantification of radiation-induced regional lung injury with perfusion imaging. *Int J Radiat Oncol Biol Phys* 1997;38:399–409.
10. Stavngaard T, Sogaard LV, Mortensen J, *et al.* Hyperpolarised 3He MRI and 81mKr SPECT in chronic obstructive pulmonary disease. *Eur J Nucl Med Mol Imaging* 2005;32:448–457.
11. Ward ER, Hedlund LW, Kurylo WC, *et al.* Proton and hyperpolarized helium magnetic resonance imaging of radiation-induced lung injury in rats. *Int J Radiat Oncol Biol Phys* 2004;58:1562–1569.
12. Marks LB, Sherouse GW, Munley MT, *et al.* Incorporation of functional status into dose-volume analysis. *Med Phys* 1999; 26:196–199.
13. Hong C, Leawoods JC, Yablonskiy DA, *et al.* Feasibility of combining MR perfusion, angiography, and 3He ventilation imaging for evaluation of lung function in a porcine model. *Acad Radiol* 2005;12:202–209.
14. Rizi RR, Saha PK, Wang B, *et al.* Co-registration of acquired MR ventilation and perfusion images—validation in a porcine model. *Magn Reson Med* 2003;49:13–18.
15. Woodhouse N, Fichele S, van Beek EJ, *et al.* A fiducial system for hyperpolarized ^{3}He/^{1}H MRI image registration [Abstract]. Presented at the UK Radiological Congress; 6–8 June 2004; Manchester, UK.
16. Das SK, Miften MM, Zhou S, *et al.* Feasibility of optimizing the dose distribution in lung tumors using fluorine-18-fluorodeoxyglucose positron emission tomography and single photon emission computed tomography guided dose prescriptions. *Med Phys* 2004;31:1452–1461.
17. Marks LB, Spencer DP, Bentel GC, *et al.* The utility of SPECT lung perfusion scans in minimizing and assessing the physiologic consequences of thoracic irradiation. *Int J Radiat Oncol Biol Phys* 1993;26:659–668.
18. Munley MT, Marks LB, Scarfone C, *et al.* Multimodality nuclear medicine imaging in three-dimensional radiation treatment planning for lung cancer: Challenges and prospects. *Lung Cancer* 1999;23:105–114.
19. Murshed H, Liu HH, Liao Z, *et al.* Dose and volume reduction for normal lung using intensity-modulated radiotherapy for advanced-stage non-small-cell lung cancer. *Int J Radiat Oncol Biol Phys* 2004;58:1258–1267.
20. Woodhouse N, Wild JM, Paley MN, *et al.* Combined helium-3/proton magnetic resonance imaging measurement of ventilated lung volumes in smokers compared to never-smokers. *J Magn Reson Imaging* 2005;21:365–369.
21. Saunders M, Dische S, Barrett A, *et al.* Continuous hyperfractionated accelerated radiotherapy (CHART) versus conventional radiotherapy in non-small-cell lung cancer: A randomised multicentre trial. CHART Steering Committee. *Lancet* 1997;350:161–165.
22. Bragg CM, Conway J, Robinson MH. The role of intensity-modulated radiotherapy in the treatment of parotid tumors. *Int J Radiat Oncol Biol Phys* 2002;52:729–738.
23. van Beek EJ, Wild JM, Fink C, *et al.* MRI for the diagnosis of pulmonary embolism. *J Magn Reson Imaging* 2003;18:627–640.
24. Wild JM, Schmiedeskamp J, Paley MN, *et al.* MR imaging of the lungs with hyperpolarized helium-3 gas transported by air. *Phys Med Biol* 2002;47:N185–N190.
25. Barber DC. Efficient nonlinear registration of 3D images using high order co-ordinate transfer functions. *J Med Eng Technol* 1999;23:157–168.
26. Ireland RH, Wood SM, Metherall P, *et al.* Feasibility of non-linear image registration for radiotherapy treatment planning with gamma camera PET [abstract]. *Nucl Med Commun* 2004;25:318.